

Single-particle and collective degrees of freedom in ^{101}Zr and $^{103,105}\text{Mo}$

R. Orlandi,^{1,*} A. G. Smith,¹ D. Patel,¹ G. S. Simpson,^{1,†} R. M. Wall,¹ J. F. Smith,¹ O. J. Onakanmi,¹ I. Ahmad,² J. P. Greene,² M. P. Carpenter,² T. Lauritsen,² C. J. Lister,² R. V. F. Janssens,² F. G. Kondev,^{2,‡} D. Seweryniak,² B. J. P. Gall,³ O. Dorveaux,³ and A. E. Stuchbery⁴

¹*University of Manchester, M13 9PL, Manchester, United Kingdom*

²*Physics Division, Argonne National Laboratory, Argonne, Illinois 60439, USA*

³*IPHC CNRS-IN2P3, ULP, F-67037 Strasbourg, France*

⁴*Department of Nuclear Physics, RSPHysSE, Australian National University, Canberra, ACT 0200, Australia*

(Received 26 September 2005; published 16 May 2006)

The g factors of several low-lying excited states of the neutron-rich ^{101}Zr and $^{103,105}\text{Mo}$ nuclei have been measured for the first time. The isotopes were produced by the spontaneous fission of a ^{252}Cf source, which was sandwiched between two magnetized iron foils and placed at the center of the Gammasphere spectrometer. The g factors of excited states of fission fragments were inferred from Larmor precessions deduced from the measurement of time-integrated perturbed angular correlation functions. The magnitude and sign of the quantity $(g_K - g_R)/Q_0$ were determined from the mixing ratios measured for the $3/2[411]$ and $5/2[532]$ rotational bands in ^{101}Zr and $^{103,105}\text{Mo}$. The combination of this quantity with the measured g factors permitted the separation of the particle-rotor parameters g_K and g_R for each band. The comparison of the extracted g_K factors to Nilsson model predictions confirms current band assignments, and this agreement is consistent with an axially symmetric picture of these nuclei at low spins. The possible effect of triaxial deformation on the measured magnetic moments was investigated in the rigid triaxial rotor-plus-particle framework. The calculations suggest that triaxial deformation plays a stronger role in the Mo than in the Zr isotopes, but that triaxiality is likely to be dynamic. The extracted g_R factors are consistently smaller than the Z/A limit, in agreement with observations in neighboring even-even nuclei.

DOI: [10.1103/PhysRevC.73.054310](https://doi.org/10.1103/PhysRevC.73.054310)

PACS number(s): 21.10.Ky, 23.20.En, 23.20.Gq, 27.60.+j

I. INTRODUCTION

A rich variety of structural phenomena characterizes the neutron-rich $A \sim 100$ region of the nuclear chart in the vicinity of ^{100}Zr . The nuclear properties of these nuclei exhibit a high sensitivity to the number of neutrons and protons, which gives rise to a wealth of rapidly changing phenomena such as the sudden spherical-to-deformed shape change experienced by Sr and Zr nuclei [1] and the emergence of triaxial degrees of freedom in the Mo and Ru isotopes [2–4].

Initially, β -decay studies offered important information on the low-lying excited states of Zr and Mo isotopes, including several lifetime measurements [5–7]. Later, γ spectroscopy of fission fragments significantly extended the knowledge on these nuclei [8–11]. Nonetheless, although more than three decades have elapsed since the first production of ^{101}Zr and $^{103,105}\text{Mo}$, their magnetic moments are still scarcely known. The only exception is the measurement of the magnetic moment of the ground state of ^{101}Zr by laser spectroscopy [12,13].

Recently, an experiment has been carried out in order to measure the g factors of states excited in secondary fission fragments, following the spontaneous fission of ^{252}Cf . The technique employed was an integrated perturbed angular

correlation (IPAC), which consisted of the measurement of the perturbative effect induced by an external magnetic field on the angular correlation function of γ -ray pairs. The mean precession of the angular correlation is proportional to the g factor of the state which is directly fed and decays via the selected pair of γ rays. The experimental technique has been described in detail in Refs. [14,15]. Some results from the experiment have already been published in Ref. [16].

In the present work, the g factors of several low-lying states in the $3/2[411]$ and $5/2[532]$ bands in ^{101}Zr and $^{103,105}\text{Mo}$ have been measured. These data, combined with a determination of the mixing ratios of several low-lying transitions, were sufficiently precise to allow separation of the single-particle from the collective contribution to the magnetic properties.

This paper is organized as follows. The experimental procedure is explained in Sec. II, and the results are presented in Sec. III. In Sec. IV, the single-particle g_K factors are compared to predictions for axially symmetric and asymmetric rotors, and the collective g_R factors are compared to predictions of the interacting boson model 2 (IBM2). A summary and conclusions are given in Sec. V.

II. EXPERIMENTAL DETAILS

Excited states in the nuclei of interest were populated following the spontaneous fission of ^{252}Cf . Their partial level schemes are shown in Figs. 1–3. The experimental details have been previously reported in Ref. [15]. γ rays emitted from the nuclei of interest were detected using the Gammasphere spectrometer [17] situated at Argonne National

*Present address: INFN - Laboratori Nazionali di Legnaro, Padova, Italy; electronic address: Riccardo.Orlandi@lnl.infn.it

†Present address: LPSC, CNRS/IN2P3, Grenoble, France.

‡Present address: Nuclear Engineering Division, ANL, Argonne, IL 60439, USA.

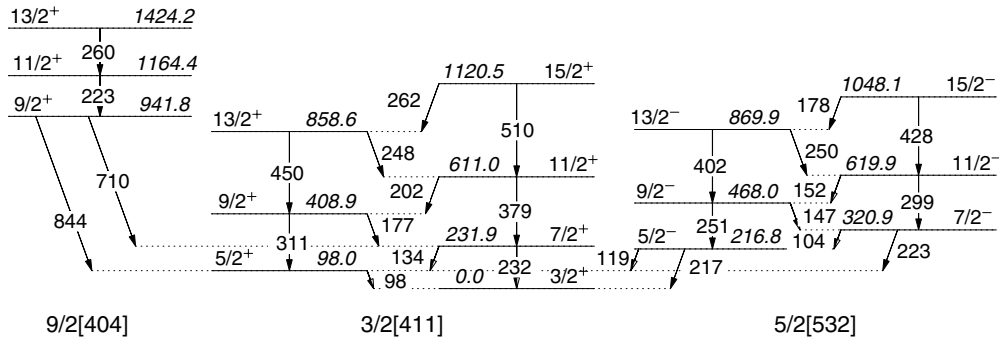


FIG. 1. Partial level scheme of ^{101}Zr from [10]. The $9/2^+$ band is from [11]. Configuration assignments are given at the bottom of each band.

Laboratory. The Gammasphere array consisted of 101, 75% efficient Compton suppressed germanium detectors. The ^{252}Cf source had a total activity of 100 μCi and a fissioning activity of 3 μCi . The source was sandwiched between two, 15 mg/cm^2 magnetized iron foils and placed at the center of the spectrometer. The fields causing the perturbation of the angular correlation functions were the hyperfine fields in the Fe foils, where the fission fragments were fully stopped. A pair of small, permanent magnets providing a magnetic field of 0.2 Tesla were placed on either side of the source. The intensity of the field was sufficient to fully magnetize the Fe foils. The magnets were mounted on a rotating support, which allowed us to reverse the direction of the field. The experiment ran for approximately 14 days, and the field direction was reversed approximately every 8 h. With the condition that three or more suppressed γ rays had to be detected before the data were accepted, a total of 9.95×10^9 events were collected.

The short implantation time of the fission fragments into the Fe foils (~ 1 ps) meant that transient field effects could be safely disregarded for states with lifetimes much longer than the stopping time; this was true for all states discussed in this work. Details about the general analysis procedures and about the Gammasphere geometry can be found in [15]. The general expression relating the mean precession angle ϕ_P to the g factor of the state is given by [18]

$$\phi_P = -\frac{gB\mu_N\tau}{\hbar}, \quad (1)$$

where B is the static hyperfine field and τ is the lifetime of the state under investigation.

We successfully identified and extracted from the data set the states of interest by selecting only those events

containing three specific transitions. These transitions or “gates” corresponded to the γ -ray line feeding the excited state, the γ ray emitted when the state decays, and a third γ ray emitted either by the same nucleus or by its complementary fragment in the fission event. The presence of the last γ ray was required only to enhance the selectivity; its direction of emission was not a factor in calculations. Extreme care was taken to ensure that the data being analyzed originated solely from the nucleus of interest and not from other, contaminant nuclei with similar spectral lines.

An indication of the selective power achieved in this work is provided by the case of the $\frac{7}{2}^-$ state in ^{105}Mo . Figure 4(a) shows a portion of the total ungated γ -ray spectrum which includes the feeding and decaying transitions of the $\frac{7}{2}^-$ state, the highlighted 138 and 95 keV lines, respectively. The histogram in Fig. 4(b) was produced by consecutively gating on these transitions in a three-dimensional γ - γ - γ cube.

The study of odd-mass isotopes was complicated by the fact that, in almost every case, at least one of the γ -ray transitions employed in each IPAC measurement was of mixed $M1/E2$ multipolarity with an unknown mixing ratio. The unperturbed angular correlation coefficients were therefore unknown and had to be determined to allow the measurement of the precession of the angular correlation functions. For the coefficients to be extracted from the data, the perturbative effect of the applied field had to be included. This was achieved by means of a nonlinear multiparameter fit, which yielded both the unperturbed angular correlation coefficients and the precession angle. This fit required a determination of the γ -ray detection efficiencies, which was accomplished following the method detailed in [15]. Validation of this procedure arose

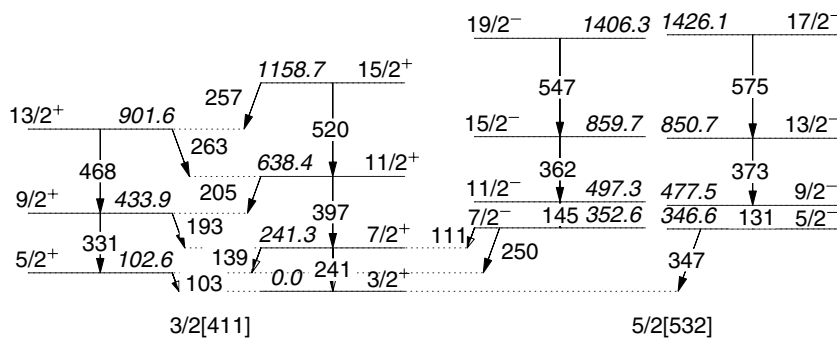


FIG. 2. Same as Fig. 1, but for ^{103}Mo from [10].

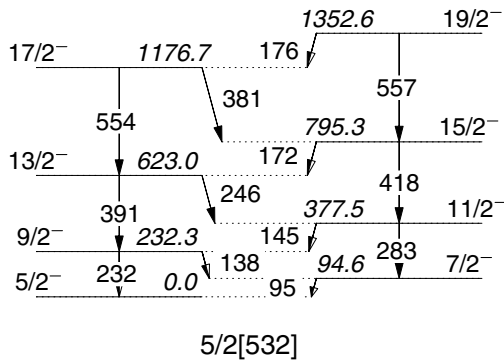


FIG. 3. Same as Fig. 1, but for ^{105}Mo from [10].

from the excellent agreement between the a_2 and a_4 angular correlation coefficients extracted with the multiparameter fit

and those recently published for various transitions in ^{101}Zr [11]. The measured a_2 and a_4 coefficients, given in Table I, were adopted for a nonlinear double-ratio analysis with ϕ_P as the only free parameter.

Whenever possible, different γ -ray pairs were used to select a single state. The $7/2^-$ state in ^{105}Mo in Fig. 3, for example, can be selected either by gating on the 138–95 or the 283–95 keV γ -ray pairs. These alternative gates lead to a completely independent determination of the precession. The consistency between these independent measurements can be seen in Table I, and it was taken as an additional confirmation of the validity of the nonlinear fit to all the data points. The g factors in Table I were derived from the weighted averages of all independent precession measurements for each state.

Once the g factors were extracted, it was possible to use the particle-rotor model definition of the g factor, together with a measurement of the mixing ratio δ , to separate the

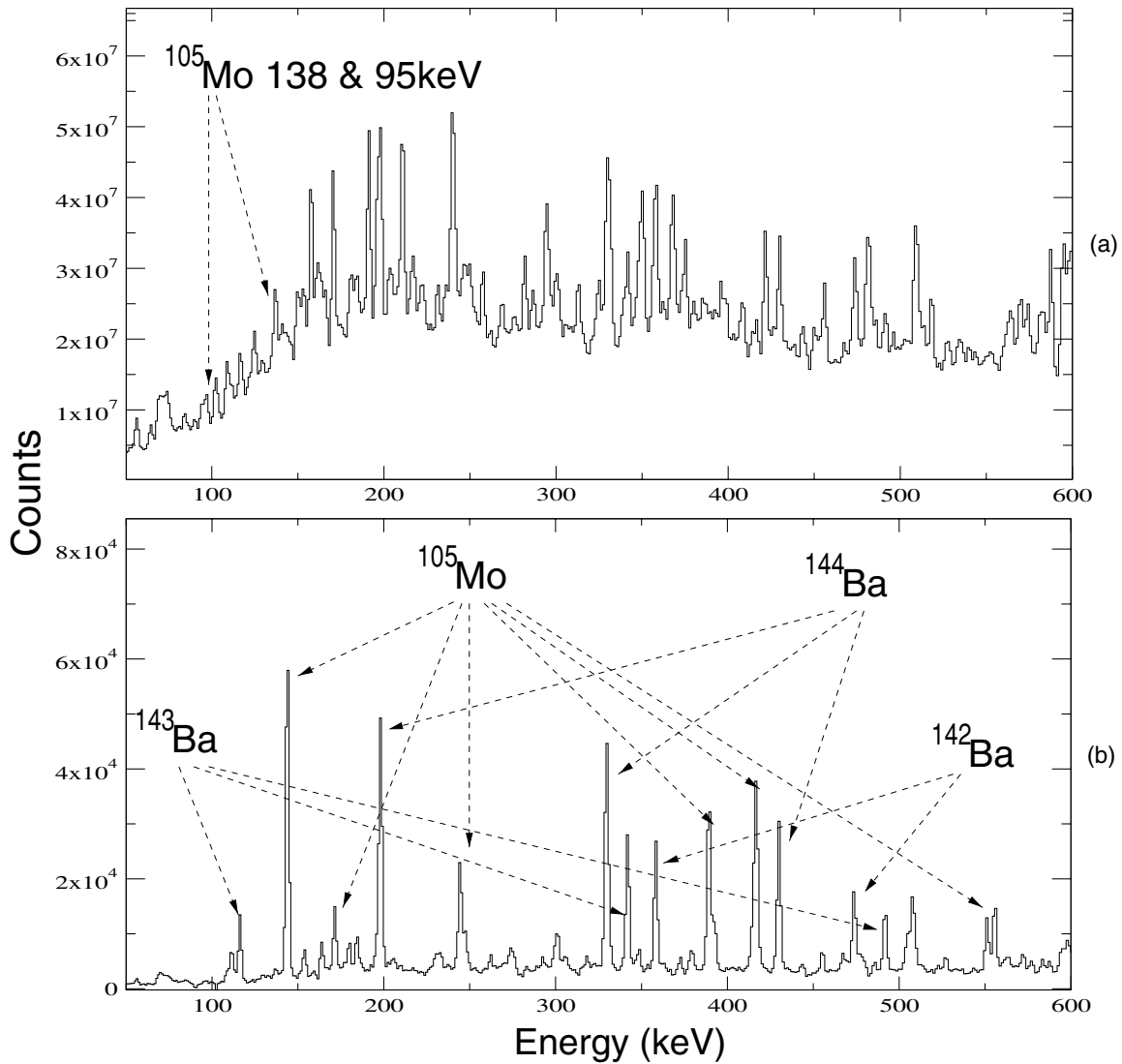


FIG. 4. (a) Portion of the total ungated γ -ray spectrum obtained from this experiment, where the feeding and decaying γ rays for the $7/2^-$ state in ^{105}Mo are indicated. (b) Spectrum produced by consecutively gating on the 138 and 95 keV lines in ^{105}Mo . Other ^{105}Mo ground-state band γ rays and intense transitions from the complementary $^{144, 143, 142}\text{Ba}$ fragments are indicated.

TABLE I. Quantities relevant to the determination of g factors for each nucleus. Each state is identified by its spin and parity I^π , excitation energy E_{exc} , and lifetime τ . The table includes the a_2 and a_4 angular correlation coefficients deduced for each independent transition (identified by the initial, intermediate, and final level) used to select each state. The g factors are determined from the weighted average of each individual precession measurement $\overline{\phi_P}$. The measured precession is also given for cases in which the lifetime was not available, since it gives a good indication of the g -factor sign. The way in which information was obtained from transitions such as $9/2^+ \rightarrow 7/2^+$ and $5/2^+ \rightarrow 3/2^+$ is described in Sec. III. The hyperfine fields assumed for Zr and Mo were, respectively, $-27.4(4)T$ [19] and $-25.60(1)T$ [20].

Nucleus	I^π, E_{exc} (keV), τ (ns)	Transition ($I_i \rightarrow I \rightarrow I_f$)	a_2	a_4	ϕ_P (mrad)	$\overline{\phi_P}$	g	
^{101}Zr	$5/2^+, 98, 0.9(3)^a$	$7/2^+ \rightarrow 5/2^+ \rightarrow 3/2^+$	0.269(12)	0.018(17)	+57(24)	+53(23)	+0.047(26)	
		$7/2^- \rightarrow 5/2^+ \rightarrow 3/2^+$	0.119(21)	-0.054(32)	+17(74)			
	$7/2^+, 232, <0.01^c$	$9/2^+ \rightarrow 7/2^+, 5/2^+ \rightarrow 3/2^+$	$9/2^+ \rightarrow 7/2^+ \rightarrow 5/2^+$	0.335(15)	0.033(22)	+63(24) ^b	+22(19)	+0.17(14)
			$9/2^+ \rightarrow 7/2^+ \rightarrow 5/2^+$	0.255(14)	0.022(20)	+14(29)		
			$11/2^+ \rightarrow 7/2^+ \rightarrow 5/2^+$	-0.175(13)	-0.022(18)	+52(39)		
	$5/2^-, 217, 0.48(17)^c$	$7/2^- \rightarrow 5/2^- \rightarrow 3/2^+$	0.136(10)	-0.010(15)	-121(43)	-121(43)	-0.19(10)	
$7/2^-, 321, 0.39(19)^c$	$9/2^- \rightarrow 7/2^- \rightarrow 5/2^-$	0.309(13)	-0.024(18)	-19(14)	-20(13)	-0.039(32)		
	$9/2^- \rightarrow 7/2^- \rightarrow 5/2^+$	0.139(19)	-0.028(28)	-26(41)				
^{103}Mo	$5/2^+, 103, 0.628(20)^d$	$7/2^+ \rightarrow 5/2^+ \rightarrow 3/2^+$	0.275(10)	-0.001(15)	+42(10)	+44(10)	+0.057(13)	
		$7/2^- \rightarrow 5/2^+ \rightarrow 3/2^+$	0.089(8)	-0.025(12)	+90(53)			
	$7/2^+, 241, 0.156(23)^d$	$9/2^+ \rightarrow 7/2^+ \rightarrow 5/2^+$	0.411(26)	-0.025(37)	-15(28)	-6(24)	-0.03(13)	
		$11/2^+ \rightarrow 7/2^+ \rightarrow 5/2^+$	-0.110(12)	0.025(17)	+18(47)			
	$7/2^-, 354, 1.73(14)^d$	$11/2^- \rightarrow 7/2^- \rightarrow 5/2^+$	-0.083(11)	-0.017(17)	-200(63)	-200(63)	-0.094(31)	
$11/2^-, 499, \text{NA}^e$	$15/2^- \rightarrow 11/2^- \rightarrow 7/2^-$	0.079(7)	0.008(11)	-134(61)	-134(61)	<0		
^{105}Mo	$7/2^-, 95, 0.69(6)^f$	$9/2^- \rightarrow 7/2^- \rightarrow 5/2^-$	-0.357(5)	0.023(8)	-55(5)	-54(5)	-0.064(8)	
		$11/2^- \rightarrow 7/2^- \rightarrow 5/2^-$	-0.129(6)	0.005(11)	-19(31)			
	$9/2^-, 234, 0.159(14)^f$	$11/2^- \rightarrow 9/2^-, 7/2^- \rightarrow 5/2^-$	$11/2^- \rightarrow 9/2^- \rightarrow 7/2^-$	0.324(9)	-0.009(13)	-62(12) ^b	-5(7)	-0.026(36)
			$11/2^- \rightarrow 9/2^- \rightarrow 7/2^-$	0.324(6)	0.012(9)	-5(9)		
			$13/2^- \rightarrow 9/2^- \rightarrow 7/2^-$	-0.114(7)	-0.003(10)	-20(33)		
$11/2^- \rightarrow 9/2^- \rightarrow 5/2^-$	-0.156(9)	0.005(14)	40(34)					

^aWeighted average of Refs. [21] and [5].

^bMeasurements *not* directly contributing to the weighted average, see Sec. III.

^cFrom Ref. [5].

^dFrom Ref. [7].

^eNot available.

^fFrom Ref. [6].

single-particle (g_K) and collective (g_R) contributions. In the particle-rotor model [22], the g factor of an axially deformed nucleus in a state of angular momentum I (with $K \neq 1/2$) is given by

$$g = g_K + (g_K - g_R) \frac{K^2}{I(I+1)}. \quad (2)$$

The single-particle g_K factor depends on the Nilsson configuration of the particle, and g_R is generated by the core. The separation of these components was achieved via the measurement of the mixing ratio δ of low-lying transitions, by exploiting the fact that δ is related to the quantity

$$\frac{(g_K - g_R)}{Q_0} = \sqrt{\frac{5}{12}} \frac{1}{K} \left(\frac{E_\gamma}{1198\delta} \right) \frac{\langle I_1 K 20 | I_2 K \rangle}{\langle I_1 K 10 | I_2 K \rangle}, \quad (3)$$

where Q_0 is the nuclear quadrupole moment, K is the projection of the total angular momentum on the symmetry axis, I_2 and I_1 are the respective initial and final states of the mixed transition, and E_γ is the γ -ray energy in keV. If the quadrupole moment is known, Eqs. (2) and (3) can be combined to determine g_K and g_R .

The mixing ratio of a transition can be determined from the measurement of the a_2 and a_4 coefficients characterizing the angular correlation between the transition of interest and another, pure one. This type of transition is exemplified by the 283–95 and 391–138 keV γ -ray pairs in ^{105}Mo . Increased precision can be gained by considering also the correlation between the 138–95 keV pair, in which both transitions are mixed (this correlation is shown in Fig. 5 as representative of the quality of our angular correlation data). The inclusion of the latter pair correlates the previous two independent angular correlation functions and provides sufficient information to

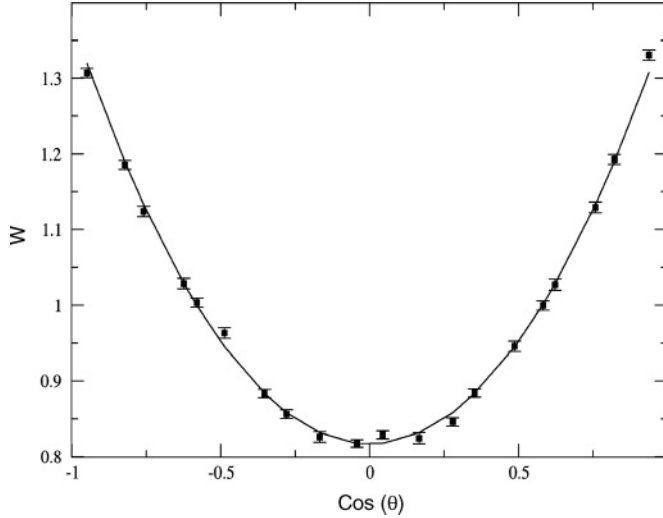


FIG. 5. Measured angular correlation function $W(\cos \theta)$ for the $9/2^- \rightarrow 7/2^- \rightarrow 5/2^-$ transitions in ^{105}Mo .

perform a nonlinear fit through all the a_2 and a_4 coefficients. In this example, a minimum in the χ^2 of the nonlinear fit corresponds to the mixing ratios of the 138 and 95 keV transitions. This procedure allows for the further inclusion of other γ -ray pairs, and as many as four mixing ratios were determined by a single fit for the same band. This fit was performed for all rotational bands in the nuclei under study for which sufficient experimental evidence was available, i.e., the only exception was the $5/2[532]$ band in ^{103}Mo . The resulting mixing ratios are listed in Table II.

III. RESULTS

Table I lists the coincidence gates associated with each precession measurement. The resulting g factors are given in the right-most column. For each state, this table also includes the lifetime.

TABLE II. Measured mixing ratios δ for the nuclei under study. For each transition, the quantity $\frac{(g_K - g_R)}{Q_0}$ is also given, in units of $\mu_N/e b$, along with the transition energy E_γ and the initial I_i and final I_f spins of the states involved.

Nucleus	E_γ (keV)	$I_i \rightarrow I_f$	δ	$\frac{(g_K - g_R)}{Q_0}$
^{101}Zr	98	$5/2^+ \rightarrow 3/2^+$	-0.112(44)	-0.36(14)
	134	$7/2^+ \rightarrow 5/2^+$	-0.253(45)	-0.147(26)
	177	$9/2^+ \rightarrow 7/2^+$	-0.133(25)	-0.282(52)
^{101}Zr	104	$7/2^- \rightarrow 5/2^-$	-0.188(21)	-0.154(17)
	147	$9/2^- \rightarrow 7/2^-$	-0.216(19)	-0.144(13)
	152	$11/2^- \rightarrow 9/2^-$	-0.183(18)	-0.143(15)
^{105}Mo	103	$5/2^+ \rightarrow 3/2^+$	-0.284(88)	-0.147(46)
	138	$7/2^+ \rightarrow 5/2^+$	-0.149(29)	-0.259(50)
^{105}Mo	95	$7/2^- \rightarrow 5/2^-$	-0.238(39)	-0.112(18)
	138	$9/2^- \rightarrow 7/2^-$	-0.225(26)	-0.130(15)
	145	$11/2^- \rightarrow 9/2^-$	-0.204(20)	-0.123(12)
	246	$13/2^- \rightarrow 11/2^-$	-0.207(18)	-0.172(15)

TABLE III. g_K and g_R values extracted in this work. Each corresponding state is labeled by its spin and parity I^π .

Nucleus	I^π	g_K	g_R	Q_0 (e b)
^{101}Zr	$5/2^+$	-0.59(15)	0.26(4)	$Q_0 = 4.1(2)$ [13]
	$5/2^-$	-0.36(11)	0.23(10)	$Q_0 = 3.9(3)$ [23]
	$7/2^-$	-0.39(6)	0.19(4)	$Q_0 = 3.9(3)$ [23]
^{103}Mo	$5/2^+$	-0.46(11)	0.23(3)	$Q_0 = 3.84(17)$ [7]
	$7/2^+$	-0.73(17)	0.09(13)	$Q_0 = 3.74(31)$ [7]
^{105}Mo	$7/2^-$	-0.36(6)	0.13(2)	$Q_0 = 4.0(1)$ [24]
	$9/2^-$	-0.42(5)	0.11(4)	$Q_0 = 4.0(1)$ [24]

For two excited states, the $7/2^+$ in ^{101}Zr and the $9/2^-$ in ^{105}Mo , Table I includes pairs of γ rays of the type $9/2^+ \rightarrow 7/2^+, 5/2^+ \rightarrow 3/2^+$, i.e., transitions connected by an additional, intermediate γ ray ($7/2^+ \rightarrow 5/2^+$ in this example). A selection made with such gates yields the measurement of the average precession over the sum-total lifetimes of the $7/2^+$ and $5/2^+$ states. It was shown by Patel *et al.* [15] that such cases provide a further precession measurement for one of the states if the mean precession undergone by the nucleus in the other state, determined with a different selection of gates, is subtracted [in this example, the $7/2^+$ state precession can be obtained by subtracting the $5/2^+$ precession measurement, 53(23) mrad]. Therefore, for these aforementioned cases, the two intermediate-state precessions given in Table I were averaged with the other measurements only after the contribution from the other state had been subtracted.

The g_K and g_R factors obtained by the combination of Eqs. (2) and (3), in the way described in Sec. II, are listed in Table III. The measured quadrupole moments are given in the right-most column. Two considerations come retrospectively in support of the validity of the g_K and g_R factor measurements. First of all, the g_K factors agree with the predictions for axially symmetric nuclei, as discussed in detail in the next section. Furthermore, as shown in Sec. IV A 2, the g_R factors follow the trend displayed by the 2^+ state g factors in their even-even neighbors, falling well below the Z/A line of the charged droplet limit. A possible explanation for the reason why the g_R factors of the odd nuclei display values significantly lower than their even-even neighbors will be given later in terms of a consequence of the fractional increase in the nuclear moment of inertia.

IV. DISCUSSION

A. Single-particle degrees of freedom

1. Axial particle-rotor model

Thanks to their sensitivity to the purity of a particular configuration, g factors, and in particular their single-particle contribution g_K , represent a stringent test of current configuration assignments. Under the assumption of axial

TABLE IV. Comparison between experimental and theoretical g_K factors of excited states in ^{101}Zr , ^{103}Mo , and ^{105}Mo . States are labeled by their spin and parity I^π . Theoretical estimates were obtained following the method outlined in Sec. IV A1.

Nucleus	I^π	g_K (exp)	g_K (theory)
^{101}Zr	$5/2^+$	-0.59(15)	-0.69(1)
	$5/2^-$	-0.36(11)	-0.36(1)
	$7/2^-$	-0.39(6)	-0.36(1)
^{103}Mo	$5/2^+$	-0.46(11)	-0.68(1)
	$7/2^+$	-0.73(17)	-0.68(1)
^{105}Mo	$7/2^-$	-0.36(6)	-0.35(1)
	$9/2^-$	-0.42(5)	-0.35(1)

symmetry, the intrinsic g_K factors can be calculated in terms of the single-particle Nilsson wave functions [25],

$$g_K = g_\ell + \frac{g_s - g_\ell}{2K} \sum_l (a_{l,K-1/2}^2 + a_{l,K+1/2}^2), \quad (4)$$

where $a_{l,K\pm 1/2}^2$ are the normalized amplitudes of the Nilsson model wave functions in the uncoupled basis [26], and g_s and g_ℓ are the intrinsic spin and orbital g factors of the unpaired nucleon. For neutrons, $g_\ell = 0$ and $g_s = 0.6g_s(\text{free})$. The values of the quantity $\sum_l (a_{l,K-1/2}^2 + a_{l,K+1/2}^2)$ for different single-particle configurations were tabulated by Browne and Femenia [27] for β deformations ranging from -0.3 to $+0.3$ in steps of 0.1 . The values assumed by this quantity at the deformations of the nuclei of interest were extrapolated from this set. The appropriate β deformations were deduced from the measured quadrupole moments listed in Table III. The uncertainty in the theoretical g_K estimates arises from the uncertainty in the measured Q_0 moments.

All the extracted g_K factors are compared to the theoretical predictions in Table IV. Very good agreement is obtained in most cases. For the $5/2^+$ state in ^{103}Mo , only reasonable agreement is observed with the predicted g_K , two standard deviations away from the g_K measured in this work.

In ^{101}Zr , the long-standing $d_{5/2} g_{7/2} 3/2[411]$ assignment [21,28,29] was recently confirmed by Thayer *et al.* [13] on the basis of a laser spectroscopy measurement of the ground-state magnetic moment. This additional measurement can be used to verify the reliability of the assumed hyperfine field. Combining the ground-state moment measured by Thayer *et al.* with the g_R value extracted in this work, and rearranging Eq. (2), the g_K factor of the $3/2^+$ state was found to be $-0.48(3)$, consistent with our measurement.

Prior to this work, the configuration assignments of none of the other bands discussed here had been tested against measured magnetic moments. There often was, however, strong indirect evidence in support of the assignments such as β -decay rates [7,30], the observation of signature splitting [8], and high-spin data [9]. The g_K factors extracted in this work confirm all previous configuration assignments. Noticeably, the agreement was obtained with predictions for axially symmetric nuclei, which did not take into account the possible presence of triaxial deformation.

This finding ought to be compared with a recent discussion by Hua *et al.* [10]: in their work, the authors have used the rigid triaxial rotor-plus-particle (RTRP) model to reproduce the observed signature splitting in the $5/2[532]$ bands in ^{101}Zr and ^{103}Mo . These authors observed that the signature splitting in ^{103}Mo is better reproduced assuming a triaxial deformation $\gamma = 19^\circ$, while the splitting in ^{101}Zr can be obtained from the model without any triaxiality. They inferred that this difference could be a manifestation of the presence of the γ degree of freedom in the molybdenum nuclei. The observation of larger triaxial deformation in ^{103}Mo than in ^{101}Zr is further supported by cranked shell model calculations performed by Skalski *et al.* [31]. Their calculations predict triaxial ground-state minima in $^{104,106,108}\text{Mo}$ and deformed prolate ground states for Zr isotopes with $60 \leq N \leq 72$.

Because of the possible discrepancy between the g factors measured in this work and the suggested triaxiality in the molybdenums, the predictive power of the RTRP model was tested against the magnetic moments measured in this work.

2. RTRP calculations

The RTRP model is described in detail by Larsson, Leander, and Ragnarsson [32]; the calculations reported here were performed using the code written by Semmes, Ragnarsson, and others [33]. The model describes a system of nucleons in which an unpaired particle is coupled to a rigid even-even core. In the present calculations, the deformed Woods-Saxon potential was used with the standard width, radius, and diffuseness parameters [33], the axial quadrupole deformation β_2 , the asymmetry parameter γ , and the hexadecapole deformation β_4 were adjusted. The range of the triaxial deformation parameter γ respects the Lund convention [34], according to which an increasing asymmetry leads the nucleus from a prolate shape for $\gamma = 0^\circ$ to an oblate shape for $\gamma = -60^\circ$.

The Hamiltonian can be written as

$$H = H_{\text{core}} + H_{\text{sp}} + H_{\text{pair}}, \quad (5)$$

where H_{sp} is the single-particle Hamiltonian in an adiabatic core field, H_{pair} is the pairing Hamiltonian, and the core Hamiltonian H_{core} has the form

$$H_{\text{core}} = \sum_{\kappa=1}^3 \frac{(I_\kappa - j_\kappa)^2}{2\mathcal{J}_\kappa}, \quad (6)$$

where I and j are the total and single-particle angular momenta, respectively. The hydrodynamic moment of inertia \mathcal{J}_κ is defined by the relation

$$\mathcal{J}_\kappa = \frac{4}{3} \mathcal{J}_0 \sin^2 \left(\gamma + \frac{2\pi\kappa}{3} \right). \quad (7)$$

The moment of inertia \mathcal{J}_0 is derived from the energy of the first 2^+ state of the core, $E(2_1^+)$, assuming rigid rotation. An initial estimate of this input parameter is obtained by averaging the $E(2_1^+)$ excitation energies of the closest neighboring even-even nuclei. Since the code does not allow for any centrifugal stretching, it is usually found that the $E(2^+)$ parameter must be adjusted to a smaller value (typically about 15% less [33]) to improve the description of the excitation energies at higher

spins. In the present calculations, which seek to reproduce both the excitation energies and the magnetic moments, the effective core 2^+ energy had to be reduced even further, in some cases by as much as 50%. The reason for this greater reduction is that in the odd- A nucleus, the Coriolis interaction induces a renormalization of the moment of inertia. Thus, as the Coriolis interactions are weakened to explain the moments, the moment of inertia must be adjusted to compensate.

The pairing interaction represented by H_{pair} is included in the model by a standard BCS calculation [32]. The Fermi level and the pairing gap are derived quantities, not adjustable parameters.

One additional model parameter, the Coriolis attenuation ξ , was introduced in the model to improve the agreement between experimental and calculated spectra. This parameter ξ can take values between 0 and 1. Its role is to reduce the strength of the Coriolis interaction by multiplying all off-diagonal matrix elements. Although theoretically no attenuation ought to be required, it has been found from extensive experience with Coriolis mixing calculations that the actual empirical matrix elements are generally about 20–50% smaller than the theoretical estimates [35]. This effect is larger for unique parity orbitals [33].

The model parameters were made to span ranges within physically justifiable limits. Usually, these ranges were deduced from experimental observables. For example, the values assumed by β_2 were deduced from the measured quadrupole moments. The limits of the g_R model parameter, also an input into the RTRP model, were consistent with the g_R values extracted in this work. Other parameters, such as γ and ξ , were allowed more freedom. A search was performed over the space defined by these parameters to find sets which could satisfactorily reproduce the experimental observables.

Initially, the RTRP model predictions were evaluated according to their ability to best reproduce the energies and ordering of the low-lying states. It was found that while the energy levels could be reproduced rather well by the RTRP model, the same could not be said for the magnetic moments. The model, in fact, displayed a tendency to provide magnetic moments much larger in magnitude than those experimentally observed. It was found that a good reproduction of the magnetic moments could only be achieved by a very significant reduction of the Coriolis attenuation. Subsequently, therefore, the predictions were ordered according to which best reproduced not only the energies of the low-lying states, but also the magnetic moments.

The comparisons between the calculated and experimental partial level schemes are presented in Figs. 6 to 10; the corresponding sets of parameters and resulting magnetic moments are summarized in Table V. For some of the bands considered, no set of parameters was found that could reproduce equally well both the energy spacings and the magnetic moments. This was true especially for the $5/2[532]$ bands. For such cases, two sets of parameters are presented, one which resulted in a good match with the observed energy spacings, labeled as set (a), and another which best reproduced the magnetic moments as set (b).

The RTRP model also yields other nuclear properties which can be used to further assess its predictive power.

$15/2^+$	1721.9	$15/2^+$	1719.8				
$13/2^+$	1421.3	$13/2^+$	1424.2	$17/2^+$	1437.5	$17/2^+$	1467.8
$11/2^+$	1160.8	$11/2^+$	1164.4	$15/2^+$	1120.5	$15/2^+$	1148.2
$9/2^+$	940.3	$9/2^+$	941.8	$13/2^+$	858.6	$13/2^+$	857.3
				$11/2^+$	611.0	$11/2^+$	611.6
				$9/2^+$	408.9	$9/2^+$	399.9
				$7/2^+$	231.9	$7/2^+$	229.1
				$5/2^+$	98.0	$5/2^+$	95.2
				$3/2^+$	0.0	$3/2^+$	0.0
		theory	exp	exp		theory	

FIG. 6. Comparison between the experimental (exp) and calculated (theory) low-lying levels in the gs band and $9/2[404]$ bands of ^{101}Zr .

Table VI compares experimental and theoretical branching ratios λ , $B(M1)/B(E2)$ ratios, and mixing ratios δ for all transitions for which this information was available. The branching and $B(M1)/B(E2)$ ratios have been extracted from the experimental data and from RTRP model predictions according to the prescriptions given in [36]. In general, it was found that the set of parameters that best reproduced the magnetic moments also reproduced satisfactorily these additional properties.

$^{101}\text{Zr } 3/2[411]$ ground-state band. The RTRP model could reproduce both the energy spacings and the magnetic moments of the ground-state band of ^{101}Zr very well. The parameters used are given in Table V. The value of β_2 is smaller than that derived from the ground-state quadrupole moment, but consistent with the value of Q_0 deduced by Smith *et al.* [23] from state lifetimes measured at higher spins. A large $\beta_4 = 0.10$ was required in order to improve the agreement between the calculations and the energies of the positive parity $9/2[404]$ band recently observed for the first time by Urban *et al.* [11]. If β_4 is small or zero, the calculated excitation energy of the $9/2[404]$ band, shown in Fig. 6, deviates from the experiment by a few hundreds of keV. It ought to be stressed, however, that the ground-state band properties could be satisfactorily reproduced also by employing smaller values of β_4 . It was also found that a Coriolis attenuation factor as low as $\xi = 0.50$ was necessary in order to predict a magnetic moment which agrees with the results presented in this work. Table VI shows that these parameters also provide a good match to the experimental λ , δ , and $B(M1)/B(E2)$ ratios. The fact that the best agreement was observed for $\gamma = 0$ supports the observations of Thayer *et al.* [13] and Hua *et al.* [10] and agrees with cranking model calculations performed by Skalski *et al.* [31], supporting axially symmetric deformation for ^{101}Zr .

$^{101}\text{Zr } 5/2[532]$ band. Similar parameters were adopted for the $5/2[532]$ band. The energy staggering present in this band was best replicated for $\gamma = -8^\circ$, as in parametric set (a) in Table V. However, this choice also places the bandhead at a much higher excitation energy of 468 keV [the bandhead

TABLE V. Input parameters for the RTRP calculations; calculated and experimental magnetic moments are compared in the right-most two columns. For each moment, given in units of μ_N , the spin and parity of the corresponding state are shown in parentheses. Theoretical level schemes obtained with these sets of parameters are shown in Figs. 6–10. A discussion of all sets of parameters is given in Sec. IV A2.

Nucleus	Band	g_R	$E_{(2^+)}$ (keV)	β_2	β_4	γ	ξ	$\mu_{th} (I^\pi)$	$\mu_{exp} (I^\pi)$
^{101}Zr	$3/2^+$	0.27	120	0.320	0.10	0.0	0.50	$-0.2716(3/2^+)$ $+0.1129(5/2^+)$ $+0.4536(7/2^+)$	$-0.272(1)(3/2^+)^a$ $+0.117(65)(5/2^+)$ $< +0.59(50)(7/2^+)$
^{101}Zr	$5/2^-$ (a)	0.30	130	0.380	0.0	-8.0	0.50	$-0.6772(5/2^-)$ $-0.5026(7/2^-)$	$-0.50(23)(5/2^-)$ $-0.14(11)(7/2^-)$
^{101}Zr	$5/2^-$ (b)	0.30	110	0.360	0.12	0.0	0.60	$-0.5650(5/2^-)$ $-0.1687(7/2^-)$	$-0.50(23)(5/2^-)$ $-0.14(11)(7/2^-)$
^{103}Mo	$3/2^+$	0.28	144	0.277	0.00	-8.0	0.66	$+0.1345(5/2^+)$ $+0.4817(7/2^+)$	$+0.143(33)(5/2^+)$ $-0.11(44)(7/2^+)$
^{103}Mo	$5/2^-$ (a)	0.20	150	0.360	0.06	-20.0	0.80	$-0.7538(7/2^-)$ $-0.4866(11/2^-)$	$-0.33(11)(7/2^-)$ $< 0 (11/2^-)$
^{103}Mo	$5/2^-$ (b)	0.15	90	0.360	0.02	-10.0	0.30	$-0.38(7/2^-)$ $-0.08(11/2^-)$	$-0.33(11)(7/2^-)$ $< 0 (11/2^-)$
^{105}Mo	$5/2^-$ (a)	0.15	140	0.360	0.02	-15.0	0.60	$-0.6154(7/2^-)$ $-0.4887(9/2^-)$	$-0.224(28)(7/2^-)$ $-0.12(16)(9/2^-)$
^{105}Mo	$5/2^-$ (b)	0.15	87	0.362	0.02	-7.0	0.24	$-0.25(7/2^-)$ $-0.0155(9/2^-)$	$-0.224(28)(7/2^-)$ $-0.12(16)(9/2^-)$

^aGround-state magnetic moment from Ref. [13].

of set (a) in Fig. 7, labeled theory (a), has been normalized to permit the comparison] and yields calculated magnetic moments much larger than those extracted in this experiment. Set (b), on the other hand, results in an excellent agreement to the magnetic moments, the bandhead excitation energy, and

the mixing, branching, and $B(M1)/B(E2)$ ratios of Table VI, at the expense of a worse reproduction of the level scheme, which at higher energies does not exhibit the observed energy staggering. As will be discussed below, similar behavior was also observed for the Mo isotopes.

TABLE VI. Comparison between experimental and theoretical values of branching ratios λ , $B(M1)/B(E2)$ ratios, and mixing ratios δ .

Nucleus	Config.	$I_i \rightarrow I_f$	E_γ	λ		$B(M1)/B(E2)$		δ	
				Exp	th (set)	Exp	th (set)	Exp	th (set)
^{101}Zr	$3/2[411]$	$7/2^+ \rightarrow 5/2^+$	134	0.45(21)	0.44	2.44(9)	2.52	$-0.112(44)$	-0.210
		$7/2^+ \rightarrow 3/2^+$	232						
		$9/2^+ \rightarrow 7/2^+$	177	0.314(86)	0.35	0.88(7)	1.00	$-0.253(45)$	-0.206
		$9/2^+ \rightarrow 5/2^+$	310						
^{101}Zr	$5/2[532]$	$9/2^- \rightarrow 7/2^-$	147	0.78(32)	0.39(a)	3.70(9)	2.03(a)	$-0.216(19)$	$-0.319(a)$
		$9/2^- \rightarrow 5/2^-$	251		0.79(b)		3.56(b)		$-0.224(b)$
		$11/2^- \rightarrow 9/2^-$	152	0.50(18)	0.41(a)	1.10(7)	0.96(a)	$-0.183(18)$	$-0.221(a)$
		$11/2^- \rightarrow 7/2^-$	299		0.55(b)		1.47(b)		$-0.219(b)$
^{103}Mo	$3/2[411]$	$7/2^+ \rightarrow 5/2^+$	103	0.41(12)	0.52	1.96(9)	2.46	$-0.149(29)$	-0.207
		$7/2^+ \rightarrow 3/2^+$	241						
^{105}Mo	$5/2[532]$	$9/2^- \rightarrow 7/2^-$	138	0.46(20)	0.24(a)	2.70(9)	1.60(a)	$-0.225(26)$	$-0.402(a)$
		$9/2^- \rightarrow 5/2^-$	232		0.59(b)		3.14(b)		$-0.239(b)$
		$11/2^- \rightarrow 9/2^-$	145	0.52(21)	0.23(a)	1.31(14)	0.62(a)	$-0.204(20)$	$-0.290(a)$
		$11/2^- \rightarrow 7/2^-$	283		0.41(b)		1.29(b)		$-0.236(b)$
		$13/2^- \rightarrow 11/2^-$	246	0.41(17)	0.14(a)	1.0(1)	0.39(a)	$-0.207(18)$	$-0.447(a)$
		$13/2^- \rightarrow 9/2^-$	391		0.35(b)		0.73(b)		$-0.235(b)$

$15/2^-$	1062.0	$15/2^-$	1048.1	$15/2^-$	1063.4
$13/2^-$	865.8	$13/2^-$	869.9	$13/2^-$	831.8
$11/2^-$	625.3	$11/2^-$	619.9	$11/2^-$	628.7
$9/2^-$	465.6	$9/2^-$	468.0	$9/2^-$	459.5
$7/2^-$	319.9	$7/2^-$	320.9	$7/2^-$	321.0
$5/2^-$	(216.8)	$5/2^-$	216.8	$5/2^-$	214.0
theory (a)		exp		theory (b)	

FIG. 7. Same as Fig. 6, but for the $5/2[532]$ band of ^{101}Zr .

The reason for the failure of the model is not obvious, but it may be linked to the following two considerations. First, the measured magnetic moments are consistent with rather pure configurations, as indicated by the overlap between the extracted g_K factors and the Browne-Femenia predictions; but a pure $5/2[532]$ configuration is unattainable in the code if $\xi \sim 1.0$, that is, without a strong reduction of the Coriolis interaction. The predicted mixing amplitudes of the K projections of the $5/2^-$ and $7/2^-$ excited states in ^{101}Zr and ^{105}Mo , respectively, are given in Table VII; the orbit numbers label the corresponding n th negative parity single-particle state calculated by the RTRP model (for $\gamma = 0$, orbit 16 corresponds to $5/2[532]$ in Nilsson notation). The better reproduction of the energy spacings resulting from each set (a) requires a stronger mixing, which is also linked to larger negative magnetic moments which deviate from our measurement. Second, the picture of a triaxial core of constant deformation may not be appropriate to reproducing the observed features, which seem more consistent with an increasing degree of triaxiality. As shown below, the results of the calculations for the Mo isotopes suggest similar conclusions.

^{103}Mo $3/2[411]$ ground-state band. The range of each parameter in Table V was limited by considerations similar to those reported for ^{101}Zr . Reasonable agreement was observed for the $7/2^+$ state magnetic moment and the $B(M1)/B(E2)$

$13/2^+$	952.7	$13/2^+$	901.6
$11/2^+$	672.5	$11/2^+$	638.4
$9/2^+$	442.6	$9/2^+$	433.9
$7/2^+$	251.4	$7/2^+$	241.3
$5/2^+$	105.0	$5/2^+$	102.6
$3/2^+$	0.0	$3/2^+$	0.0
theory		exp	

FIG. 8. Same as Fig. 6, but for the gs band of ^{103}Mo .

and mixing ratios. A γ deformation of -8° was required to minimize the deviation of the $7/2^+$ magnetic moment from the measured value, without any dramatic change in the level spacings. Although the agreement is not as remarkable as for the $3/2[411]$ band in ^{101}Zr , the larger γ value required by the calculations may point toward a shape which is softer with respect to triaxial deformation.

^{103}Mo $5/2[532]$ band. The set of parameters (a) reported in Table V reproduced the low-spin energy spacings reasonably well. The value of γ is very close to the one which can be deduced from the $E(2_2^+)/E(2_1^+)$ ratio in ^{104}Mo and ^{106}Mo and employed by Hua *et al.* [10] in their RTRP calculations. The extreme sensitivity of the ^{103}Mo band to the Coriolis attenuation parameter did not allow any significant reduction of ξ without a dramatic change in the energy spacings. Parameters very similar to those which reproduced the magnetic moment of ^{105}Mo were employed in ^{103}Mo as a test. These parameters, corresponding to set (b) in Table V, yield a very poor match to the energy spacings. In fact, they predict the level scheme labeled “theory (b)” in Fig. 10, which is almost identical to the one found for ^{105}Mo . This alternative choice of parameters, however, results in a rather pure $5/2[532]$ configuration and a good match for the measured magnetic moments.

TABLE VII. Calculated mixing amplitudes vs K projections of the single-particle orbits which determine the $5/2^-$ and $7/2^-$ states in ^{101}Zr and ^{105}Mo , respectively. Mixing amplitudes are given for sets (a) and (b) in Table V.

Nucleus	Level	Set	K				
			Orbit No.	5/2	1/2	-3/2	-7/2
^{101}Zr	$5/2^-$	(a)	15	-0.002	0.006	-0.213	—
			16	-0.976	-0.002	0.001	—
		(b)	15	—	—	0.089	—
			16	0.996	—	—	—
^{105}Mo	$7/2^-$	(a)	14	0.003	-0.055	0.029	-0.004
			15	0.002	-0.049	-0.255	0.023
			16	-0.942	-0.036	-0.005	0.001
		(b)	17	-0.002	-0.001	0.017	-0.195
			15	0.000	-0.002	-0.060	0.002
			16	0.998	0.005	0.000	0.000

					15/2 ⁻ 1105.2
				13/2 ⁻ 898.6	
13/2 ⁻ 806.1	15/2 ⁻ 865.6	15/2 ⁻ 859.7	13/2 ⁻ 850.7		11/2 ⁻ 719.5
				9/2 ⁻ 566.9	
9/2 ⁻ 469.5	11/2 ⁻ 513.1	11/2 ⁻ 497.3	9/2 ⁻ 477.5		7/2 ⁻ 443.3
5/2 ⁻ (346.6)	7/2 ⁻ 346.7	7/2 ⁻ 352.6	5/2 ⁻ 346.6	5/2 ⁻ (346.6)	
theory (a)		exp			theory (b)

FIG. 9. Same as Fig. 6, but for the 5/2[532] band of ¹⁰³Mo.

¹⁰⁵Mo 5/2[532] ground-state band. To reproduce the magnetic moments, the Coriolis attenuation parameter had to be reduced to 0.24. The effects on the mixing amplitudes of the 7/2⁻ state are illustrated in Table VII for $\xi = 0.60$ and $\xi = 0.24$. Again, the measured magnetic moments are consistent with a very pure 5/2[532] configuration. This set of parameters [set (b) in Table V] also predicts the branching, mixing, and $B(M1)/B(E2)$ ratios of Table VI which agree with the data. As for the bands in ¹⁰³Mo, larger mixing and triaxial deformation are required to reproduce the staggering observable in the partial level schemes presented in Fig. 10. This behavior, coupled to the agreement between our measurements and the predictions for axially symmetric nuclei, again suggest that triaxiality in ^{103,105}Mo (and possibly in the 5/2[532] band in ¹⁰¹Zr) may be dynamic in character. The RTRP model, which allows only for a constant triaxial deformation, should not be expected to reproduce all of their nuclear properties. These results also warn against inferring nuclear electromagnetic properties from the RTRP model, if the only requirement is a good reproduction of the energy spacings. The present work shows, however, that if other experimental observables are well reproduced, such as branching and $B(M1)/B(E2)$ ratios, the predicted magnetic moments will more likely be correct.

B. Collective degrees of freedom

The collective gyromagnetic ratio g_R is related to the magnetic properties associated with the core. In the limit of a uniformly charged droplet, $g_R \simeq Z/A$. In reality, however,

15/2 ⁻ 781.5	15/2 ⁻ 795.3	15/2 ⁻ 786.0
13/2 ⁻ 617.3	13/2 ⁻ 623.0	13/2 ⁻ 572.0
11/2 ⁻ 379.9	11/2 ⁻ 377.5	11/2 ⁻ 386.0
9/2 ⁻ 230.5	9/2 ⁻ 232.3	9/2 ⁻ 228.8
7/2 ⁻ 92.6	7/2 ⁻ 94.6	7/2 ⁻ 100.1
5/2 ⁻ 0.0	5/2 ⁻ 0.0	5/2 ⁻ 0.0
theory (a)	exp	theory (b)

FIG. 10. Same as Fig. 6, but for the gs band of ¹⁰⁵Mo.

this limit is rarely observed, and deviations from this ratio were predicted as early as 1968 by Prior, Boehm, and Nilsson [37].

The g_R values extracted in this work are summarized in Table III. The new measurements are significantly smaller than the Z/A limit, a property also displayed by the g factors of the 2⁺ states of neighboring even-even isotopes. In Fig. 11, the weighted averages of the collective g factors extracted in this work for each nucleus have been plotted together with the 2⁺-state g factors of close-lying, even-even isotopes. Other data points refer to measurements obtained from different experiments and to g factors measured by Patel [14].

Together with the Z/A limit, Fig. 11 also presents previous fits to IBM2 parameters by Smith *et al.* [16] for two different sets of proton- and neutron-bosons g factors, g_π and g_ν . Reasonable agreement between theory and experiment is observed either for $(g_\pi, g_\nu) = (0.65, 0.05)$ or $(1.0, -0.1)$. Because, to first approximation, g_π should be a function of proton number only, and since a choice of $g_\pi \approx 1$ and $g_\nu \approx 0$ gives consistency with IBM2 fits in other regions of the nuclear chart, Smith *et al.* [16] found it preferable to suppose that the

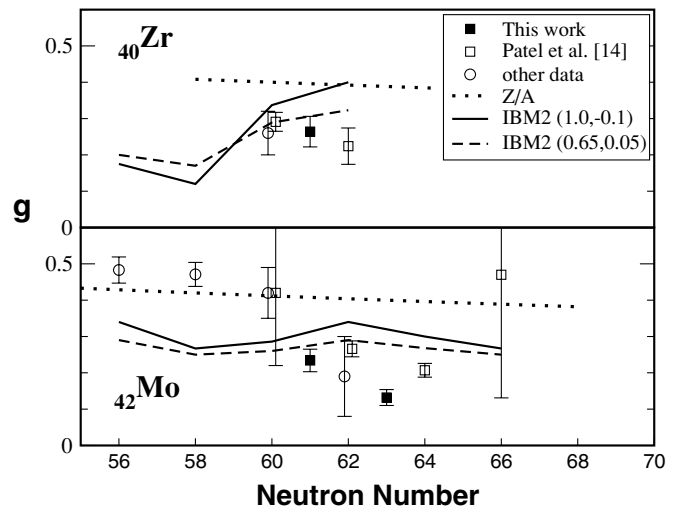


FIG. 11. g_R values extracted in this work, together with a summary of previously measured 2⁺ state g factors, either from the same data set by Patel [14] or by other authors from independent experiments. All other measurements are referenced in [16]. Experimental results are compared to the Z/A limit and to IBM2 predictions for different values of proton- and neutron-boson g factors (g_π, g_ν) given in the legend.

marked variation of the g factors with neutron number is a result of a small change in g_v . They suggest that the shift to negative values of g_v may be taken as an indication of the filling of low- Ω , $h_{11/2}$ single-particle orbitals that couple to give a 2^+ state with a negative g factor.

The IBM2 fits to the data, however, do not reproduce the observed deviation with the neighboring g factors exhibited by the present measurements. Bohr and Mottelson [38] argued that, in general, the difference between the g_R factor of rotational odd- A nuclei and their even-even neighbors is to be ascribed to their larger moments of inertia. For an odd- N nucleus, such a deviation is given by

$$\delta g_R \approx -\frac{\delta \mathcal{J}}{\mathcal{J}} g_R, \quad (8)$$

where \mathcal{J} is the moment of inertia of the $A - 1$, even-even neighbour, and $\delta \mathcal{J}$ the observed difference. This ratio should, however, be taken only as a rough estimate of the magnitude of this effect.

A theoretical estimate of δg_R can be obtained if $\delta \mathcal{J}$ can be extracted from the observed excitation energies in the nucleus of interest and in the neighboring even-even nuclei. $\delta \mathcal{J}$ refers to the difference in the collective moments of inertia. This quantity becomes difficult to estimate if a large single-particle alignment is present in the odd-mass nucleus (as is the case for bands which originate from the spherical $h_{11/2}$ orbital). This would lead the nucleus to a larger effective moment of inertia, arising both from the collective and the single-particle aligned angular momenta. An estimate of the aligned angular momentum is usually obtained by adopting the neighboring even-even nucleus as a reference frame. The adoption of such a frame of reference would, however, obviously imply that $\delta g_R = 0$. Although not immediately applicable, Eq. (8) points in the right direction, predicting smaller g_R for ^{101}Zr , ^{103}Mo , and ^{105}Mo in reference to, respectively, ^{100}Zr , ^{102}Mo , and ^{104}Mo even-even cores.

V. CONCLUSIONS

The g factors of several excited states in ^{101}Zr , ^{103}Mo , and ^{105}Mo have been measured. The fragments were obtained from the spontaneous fission of ^{252}Cf . The measurements were performed with the Gammasphere spectrometer, following the technique described in [15]. The additional determination of the mixing ratios, combined with the measured g factors, permitted the isolation of the single-particle and collective contributions to the magnetic moments.

The extracted g_K factors confirm the current band assignments as they match the predictions for axially symmetric nuclei. Calculations were also performed within the framework of the RTRP model. The comparisons with the measured magnetic properties of the low-spin states suggest that triaxial deformation plays a stronger role in the Mo than in the Zr isotopes, but that triaxiality is likely to be dynamic in nature. More data, especially at higher spins, are necessary, however, to confirm this hypothesis.

The g_R factors, consistently smaller than the Z/A limit, exhibit a trend similar to that displayed by their even-even neighbors and support the results of previous IBM2 calculations. Differences between even and odd isotopes have been tentatively explained in terms of a change in the moments of inertia.

ACKNOWLEDGMENTS

The authors would like to acknowledge J. A. Pinston and A. Scherillo for stimulating discussions and enlightening comments. The authors are also indebted for the use of the ^{252}Cf source to the Office of Basic Energy Sciences, U.S. Department of Energy, through the transplutonium element production facilities at the Oak Ridge National Laboratory. This project was supported by the UK EPSRC and the U.S. Department of Energy, Office of Nuclear Physics, under Contract No. W-31-109-ENG-38 (ANL).

-
- [1] P. Federman and S. Pittel, Phys. Rev. C **20**, 820 (1979).
 [2] A. Guessous, N. Schulz, W. R. Phillips, I. Ahmad, M. Bentaleb, J. L. Durell, M. A. Jones, M. Leddy, E. Lubkiewicz, L. R. Morss, R. Piepenbring, A. G. Smith, W. Urban, and B. J. Varley, Phys. Rev. Lett. **75**, 2280 (1995).
 [3] A. Guessous, N. Schulz, M. Bentaleb, E. Lubkiewicz, J. L. Durell, C. J. Pearson, W. R. Phillips, J. A. Shannon, W. Urban, B. J. Varley, I. Ahmad, C. J. Lister, L. R. Morss, K. L. Nash, C. W. Williams, and S. Khazrouni, Phys. Rev. C **53**, 1191 (1996).
 [4] A. G. Smith, J. L. Durell, W. R. Phillips, M. A. Jones, M. Leddy, W. Urban, B. J. Varley, I. Ahmad, L. R. Morss, M. Bentaleb, A. Guessous, E. Lubkiewicz, N. Schulz, and R. Wyss, Phys. Rev. Lett. **77**, 1711 (1996).
 [5] G. Lhersonneau, H. Gabelmann, M. Liang, B. Pfeiffer, K. L. Kratz, and H. Ohm (ISOLDE Collaboration), Phys. Rev. C **51**, 1211 (1995).
 [6] M. Liang, H. Ohm, U. Paffrath, B. De Sutter, and K. Sistemich, in KFA–IKP Ann. Rep., 1991, p. 16.
 [7] M. Liang, H. Ohm, I. Ragnarsson, and K. Sistemich, Z. Phys. A **346**, 101 (1993).
 [8] M. A. C. Hotchkis, J. L. Durell, J. B. Fitzgerald, A. S. Mowbray, W. R. Phillips, I. Ahmad, M. P. Carpenter, R. V. F. Janssens, T. L. Khoo, E. F. Moore, L. R. Morss, P. Benet, and D. Ye, Nucl. Phys. **A530**, 111 (1991).
 [9] J. K. Hwang, A. V. Ramayya, J. H. Hamilton, L. K. Peker, J. Kormicki, B. R. S. Babu, T. N. Ginter, C. J. Beyer, G. M. Ter-Akopian, Y. T. Oganessian, A. V. Daniel, W. C. Ma, P. G. Varmette, J. O. Rasmussen, S. J. Asztalos, S. Y. Chu, K. E. Gregorich, A. O. Macchiavelli, R. W. Macleod, J. Gilat, J. D. Cole, R. Aryaeinejad, K. Butler-Moore, M. W. Drigert, M. A. Stoyer, L. A. Bernstein, R. W. Loughheed, K. J. Moody, S. G. Prussin, H. C. Griffin, and R. Donangelo, J. Phys. G **24**, L9 (1998).
 [10] H. Hua, C. Y. Wu, D. Cline, A. B. Hayes, R. Teng, R. M. Clark, P. Fallon, A. Goergen, A. O. Macchiavelli, and K. Vetter, Phys. Rev. C **69**, 014317 (2004).

- [11] W. Urban, J. A. Pinston, J. Genevey, T. Rzaca-Urban, A. Zlomaniec, G. Simpson, J. L. Durell, A. G. Phillips, W. R. Smith, B. J. Varely, I. Ahmad, and N. Schulz, *Eur. Phys. J. A* **22**, 241 (2004).
- [12] P. Campbell, H. L. Thayer, J. Billowes, P. Dendooven, K. T. Flanagan, D. H. Forest, J. A. R. Griffith, J. Huikari, A. Jokinen, R. Moore, A. Nieminen, G. Tungate, S. Zemlyanoi, and J. Äystö, *Phys. Rev. Lett.* **89**, 082501 (2002).
- [13] H. L. Thayer, J. Billowes, P. Campbell, P. Dendooven, K. T. Flanagan, D. H. Forest, J. A. R. Griffith, J. Huikari, A. Jokinen, R. Moore, A. Nieminen, G. Tungate, S. Zemlyanoi, and J. Äystö, *J. Phys. G* **29**, 2247 (2003).
- [14] D. Patel, Ph.D. thesis, University of Manchester 2003.
- [15] D. Patel, A. G. Smith, G. S. Simpson, R. M. Wall, J. F. Smith, O. J. Onakanmi, I. Ahmad, J. P. Greene, M. P. Carpenter, T. Lauritsen, C. J. Lister, R. F. Janssens, F. G. Kondev, D. Seweryniak, B. J. P. Gall, O. Dorveaux, and B. Roux, *J. Phys. G* **28**, 649 (2002).
- [16] A. G. Smith, D. Patel, G. S. Simpson, R. M. Wall, J. F. Smith, O. J. Onakanmi, I. Ahmad, J. P. Greene, M. P. Carpenter, T. Lauritsen, C. J. Lister, R. V. F. Janssens, F. G. Kondev, D. Seweryniak, B. J. P. Gall, O. Dorveaux, and B. Roux, *Phys. Lett.* **B591**, 55 (2004).
- [17] P. J. Nolan, F. A. Beck, and D. B. Fossan, *Annu. Rev. Nucl. Part. Sci.* **45**, 561 (1994).
- [18] K. Recknagel, *Nuclear Spectroscopy and Reactions*, edited by J. Cerny (Academic, New York, 1974).
- [19] A. R. Arends and F. Pleiter, *Hyp. Int.* **7**, 361 (1979).
- [20] R. H. Dean and G. A. Jakins, *J. Phys. F* **8**, 1563 (1978).
- [21] H. Ohm, G. Lhersonneau, U. Paffrath, K. Shizuma, and K. Sistemich, *Z. Phys. A* **326**, 233 (1987).
- [22] A. Bohr and B. R. Mottelson, *Mat. Fys. Medd. Dan. Vid. Selsk.* **27**(16), 1 (1953).
- [23] A. G. Smith, G. S. Simpson, J. Billowes, J. D. Durell, W. R. Phillips, P. J. Dagnall, S. J. Freeman, M. Leddy, A. A. Roach, J. F. Smith, A. Jungclaus, K. P. Lieb, C. Teich, N. Schulz, B. J. P. Gall, F. Hoellinger, I. Ahmad, J. Greene, and A. Algora, in *Nuclear Structure 98, Gatlinburg, TN, 1998*, AIP Conf. Proc. 481, edited by C. Baktash (AIP, New York, 1999), p. 283.
- [24] M. Liang, H. Ohm, B. De Sutter-Pomme, and K. Sistemich, *Z. Phys. A* **351**, 13 (1995).
- [25] K. E. G. Loebner, in *The Electromagnetic Interaction in Nuclear Spectroscopy*, edited by W. D. Hamilton (North-Holland, Amsterdam, 1975), p. 141.
- [26] S. G. Nilsson, *Mat. Fys. Medd. Dan. Vid. Selsk.* **29**(16) (1955).
- [27] E. Browne and F. R. Femenia, *Nucl. Data Tables* **10**, 81 (1971).
- [28] F. K. Wohn, J. C. Hill, R. F. Petry, H. Dejbakhsh, Z. Berant, and R. L. Gill, *Phys. Rev. Lett.* **51**, 873 (1983).
- [29] M. A. C. Hotchkis, J. L. Durell, J. B. Fitzgerald, A. S. Mowbray, W. R. Phillips, I. Ahmad, M. P. Carpenter, R. V. F. Janssens, T. L. Khoo, E. F. Moore, L. R. Morss, P. Benet, and D. Ye, *Phys. Rev. Lett.* **64**, 3123 (1990).
- [30] G. Lhersonneau, P. Dendooven, A. Honkanen, M. Huhta, M. Oinonen, H. Penttilä, J. Äystö, J. Kurpeta, J. R. Persson, and A. Popov, *Phys. Rev. C* **54**, 1592 (1996).
- [31] J. Skalski, S. Mizutori, and W. Nazarewicz, *Nucl. Phys.* **A617**, 282 (1997).
- [32] S. E. Larsson, G. Leander, and I. Ragnarsson, *Nucl. Phys.* **A307**, 189 (1978).
- [33] P. Semmes and I. Ragnarsson, *The Particle plus Triaxial Rotor Model: A User's Guide*, distributed at the Hands-on Nuclear Physics Workshop, Oak Ridge, TN, 5–16 August, 1991 (unpublished).
- [34] G. Andersson, S. E. Larsson, G. Leander, P. Möller, S. G. Nilsson, I. Ragnarsson, S. Åberg, R. Bengtsson, J. Dudek, B. Nerlo-Pomorska, K. Pomorski, and Z. Szymanski, *Nucl. Phys.* **A268**, 205 (1976).
- [35] R. F. Casten, *Nuclear Structure from a simple perspective* (Oxford University, Oxford, 1990).
- [36] I. Stefanescu, J. Eberth, G. de Angelis, N. Warr, G. Gersch, T. Steinhardt, O. Thelen, D. Weisshaar, T. Martinez, A. Jungclaus, R. Schwengner, K. P. Lieb, E. A. Stefanova, D. Curien, and A. Gelberg, *Phys. Rev. C* **69**, 034333 (2004).
- [37] O. Prior, F. Boehm, and S. G. Nilsson, *Nucl. Phys.* **A110**, 257 (1968).
- [38] A. Bohr and B. R. Mottelson, *Nuclear Structure* (Benjamin, New York, 1975), Vol. 2.